Biophysics and Physicobiology

Review Article (Invited)

Biochemical and crystallographic studies of monomeric and dimeric bovine cytochrome *c* oxidase

Kyoko Shinzawa-Itoh and Kazumasa Muramoto

Graduate School of Science, University of Hyogo, 3-2-1 Kouto, Kamigori, Ako, Hyogo 678-1297, Japan

Cytochrome *c* oxidase (CcO), a terminal oxidase in the respiratory chain, catalyzes the reduction of O_2 to water coupled with the proton pump across the membrane. Mitochondrial CcO exists in monomeric and dimeric forms, and as a monomer as part of the respiratory supercomplex, although the enzymatic reaction proceeds in the CcO monomer. Recent biochemical and crystallographic studies of monomeric and dimeric CcOs have revealed functional and structural differences among them. In solubilized mitochondrial membrane, the monomeric form is dominant, and a small amount of dimer is observed. The activity of the monomeric CcO is higher than that of the dimer, suggesting that the monomer is the active form. In the structure of monomeric CcO, a hydrogen bond network of water molecules is formed at the entrance of the proton transfer K-pathway, and in dimeric CcO, this network is altered by a cholate molecule binding between monomers. The specific binding of the cholate molecule at the dimer interface suggests that the binding of physiological ligands similar in size or shape to cholate could also trigger dimer formation as a physiological standby form. Because the dimer interface also contains weak interactions of nonspecifically bound lipid molecules, hydrophobic interactions between the transmembrane helices, and a Met–Met interaction between the extramembrane regions, these interactions could support the stabilization of the standby form. Structural analyses also suggest that hydrophobic interactions of cardiolipins bound to the transmembrane surface of CcO are involved in forming the supercomplex.

Key words: mitochondria, respiratory chain, complex IV, lipid, cholate

Corresponding authors: Kyoko Shinzawa-Itoh, Graduate School of Science, University of Hyogo, 3-2-1 Kouto, Kamigori, Ako, Hyogo 678-1297, Japan. e-mail: shinzawa@sci.u-hyogo.ac.jp; Kazumasa Muramoto, Graduate School of Science, University of Hyogo, 3-2-1 Kouto, Kamigori, Ako, Hyogo 678-1297, Japan. e-mail: muramoto@sci.u-hyogo.ac.jp

Introduction

Cellular respiration is a fundamental process that generates energy in organisms. The process includes several redox reactions catalyzed by membrane proteins to oxidize the reduced electron carriers, such as NADH. This series of the proteins and carriers is called the electron transport chain or the respiratory chain. Many organisms, including humans, use the oxidation power of O_2 as the final oxidant in aerobic respiration. Aerobic respiration consumes most

---

◀ *Significance* ▶

Structural analyses of mitochondrial CcO have been based on the crystal structure of dimeric form. However, recent studies have revealed the structures of the monomeric form and of the monomer in the respiratory supercomplex. Characterization of the three states of CcO (the independent monomer, the monomer in the supercomplex, and the dimer) and structural and functional comparison of monomeric and dimeric CcOs suggest the mechanism of dimerization and supercomplex formation, and imply that the three states are in equilibrium and transition among these states regulates respiratory electron transport activity.
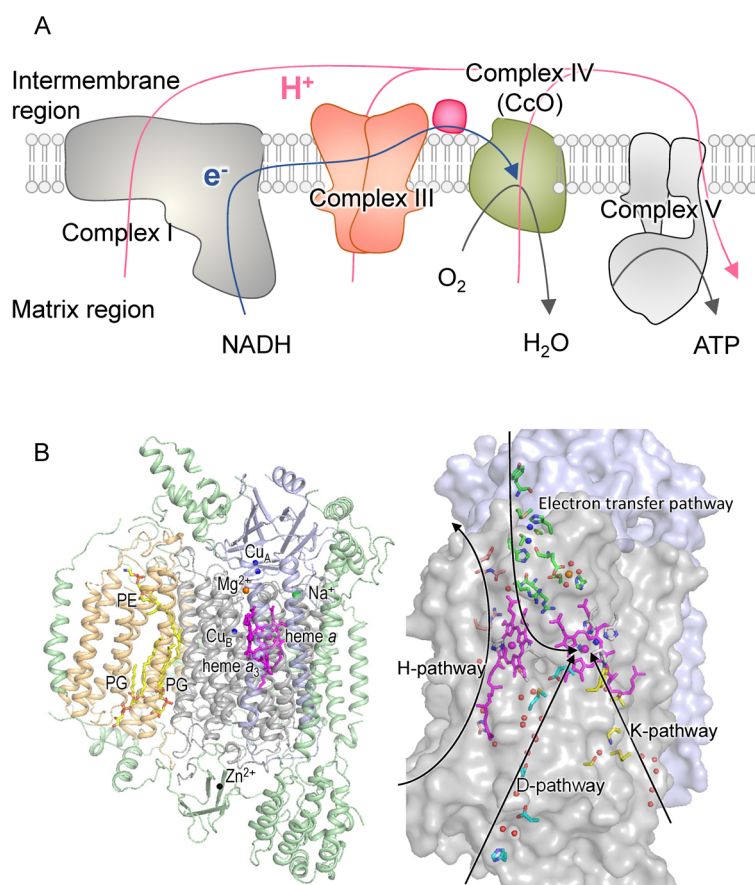
Figure 1 (A) Mitochondrial respiratory chain. Complex I: NADH-ubiquinone oxidoreductase or NADH dehydrogenase. Complex III: ubiquinol-cytochrome *c* oxidoreductase or cytochrome bc_1 complex. Complex IV: ferrocytochrome *c*-O_2 oxidoreductase or CcO. Complex V: F-type ATP synthase. e^- and H^+ are electrons and protons, respectively. (B) Structure of CcO. Subunits I, II, III, and other subunits are shown in gray, light blue, light orange, and green, respectively.

of the O_2 taken into the organism. In some bacteria, NO_3^-, SO_4^{2-}, or CO_2 are used as oxidants instead of O_2 in anaerobic respiration. The electron transport in respiration is coupled with active proton transport across the biological membrane, generating the proton gradient (the proton-motive force). This electro-chemical potential energy drives ATP synthesis using ADP and inorganic phosphate via oxidative phosphorylation. In many eukaryotes, respiratory electron transport and oxidative phosphorylation occur in the inner membranes of mitochondria, which are the power plants of the cell (Fig. 1A). The respiratory chain in mitochondria consists of large membrane protein complexes, complex I, complex III, complex IV, and complex V, which is ATP synthase. These complexes have been characterized in many structural and functional studies.

Respiratory complex IV, also known as cytochrome *c* oxidase (CcO), catalyzes the reduction of O_2 to water coupled with the proton pump across the membrane. Mitochondrial CcO consists of core subunits I, II, and III coded by mitochondrial genes, and several peripheral subunits coded by nuclear genes. Figure 1B shows the whole structure of bovine mitochondrial CcO, in which 10 nuclear-coded subunits (IV, Va, Vb, VIa, VIb, VIc, VIIa, VIIb, VIIc, and VIII) are associated with the core subunits. Since the first crystal structure was determined at 2.8 Å resolution in 1996 [1], the resolution of bovine CcO structure has been improved to 1.3 Å [2]. The transmembrane region of subunit I contains two hemes (hemes *a* and a_3) and a copper atom (Cu_B), and heme a_3 and Cu_B form the O_2 reduction site [3–5]. The extramembrane domain of subunit II contains the dinuclear copper (Cu_A) site. The electrons are transferred from ferrocytochrome *c*, which is bound to the hydrophilic surface of subunit II, to the O_2 reduction site through Cu_A and heme *a* [6]. The protons used for the O_2 reduction are transferred from the matrix region of mitochondria through two hydrogen bond networks (K- and D-pathways) in the transmembrane region of subunit I [7,8]. Substrate O_2 is transferred from the membrane region through the hydrophobic channel in the transmembrane region of subunits III and I [9]. Product water molecules may be transferred out via a route other than the O_2 channel [10]. The proton pump from the matrix

region to the inter-membrane region occurs through subunit I. Another hydrogen bond network (H-pathway) has been proposed for the proton pump in bovine CcO [11,12], although the D-pathway is thought to be used in yeast mitochondrial CcO [13].

Mitochondrial CcO is a member of the heme-copper oxygen reductase (HCOR) superfamily, which is subdivided into A-type, B-type, and C-type oxygen reductases used in aerobic and microaerobic respiration, and nitric oxide reductases (NORs) used in anaerobic respiration [14,15]. A-type HCORs are present in bacteria, archaea, and eukaryota, B-type HCORs and NORs are present in bacteria and archaea, and C-type HCORs are only found in bacteria. The functional unit of all known HCORs is a monomer, whereas there is also a dimeric form in bacterial quinol-dependent NORs [16,17]. Bovine CcO exists as monomeric and dimeric forms [18,19], although only the monomeric forms are known for other A-type HCOR members. Structural analysis by cryo-electron microscopy has revealed the supercomplex forms of CcO from mammals, yeast, and bacteria [20–24], in which monomeric CcO is associated with complexes I and III or with complex III alone. Accordingly, each of monomeric, dimeric, and supercomplex states of CcO may play a functional role in the physiological environment [25–30]; however, functional differences in CcO among these states based on the structure remain to be elucidated. In this review article, we describe the biochemical analysis of the transition between monomeric and dimeric states, and the structural and functional comparison of the monomeric and dimeric forms of bovine CcO.

Biochemical characterization of monomeric and dimeric CcO

For structural and functional analysis, it is necessary to prepare CcO samples with high purity and yield. We have been improving the method of purifying CcO from the mitochondria of bovine heart muscle for many years. The purification method consists of three main processes. (1) Preparation of Keilin–Hartree submitochondrial particles (KHPs) from the muscle cell homogenate by acid precipitation. (2) Solubilization of KHPs using cholate and fractionation by ammonium sulfate (AS) precipitation. (3) Replacement of cholate with alkyl glycoside detergents and sample washing by dialysis and ultrafiltration. Each step in these processes causes the transition of CcO between monomeric and dimeric states depending on the concentrations of CcO, cholate, and detergent, and on the pH of the solution. The relation between each purification step, CcO state, and cholate amount is summarized as follows (details of purification methods are described in [2,8]). During the following processes, 100 mM sodium phosphate (Na-Pi), pH 7.4 is used for a solvent buffer unless otherwise noted, and the temperature is maintained at 0–4°C as far as possible.

Bovine heart muscle from which fat and connective tissues are removed, is minced and 1100 g is suspended in 20 mM Na-Pi. After homogenization by blade homogenizer, mitochondria are broken into KHPs. The KHPs are collected in the supernatant after centrifuging, and then are aggregated by acetic acid treatment to decrease the pH to 5.15. The precipitated KHPs are centrifuged and suspended in 576 mL buffer before being stored. During the characterization of CcO in KHPs, when the KHPs are solubilized using detergents, digitonin (Fig. 2A, lane 1), and n-decyl-β-$_D$-maltoside (DM) (Fig. 2A, lane 2), these solutions contain substantial amounts of CcO
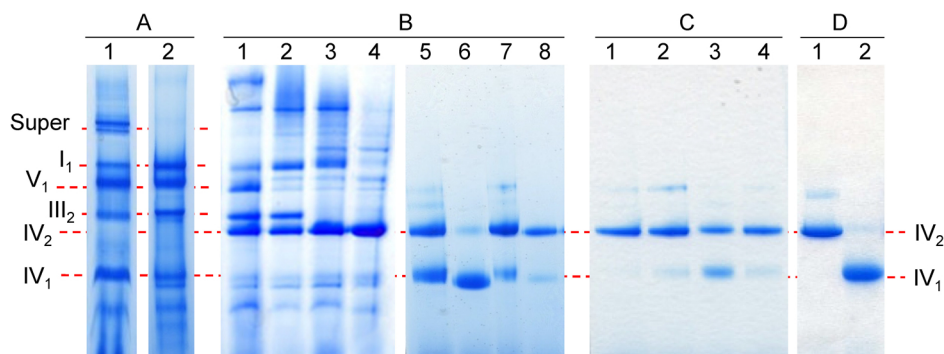

Figure 2 Blue native PAGE technique, developed by Schägger and von Jagow that uses Coomassie G-250 as a charge-shift molecule [31], can be used to determine native protein masses and oligomeric states and to identify physiological protein–protein interactions. (A) Solubilized mitochondrial membrane samples. (B) Samples from the CcO purification process. Panels A and B reproduced from [2]. (C) CcO samples purified under different conditions. (D) CcO samples stabilized with amphipols. Panels C and D reproduced from [8]. The experimental conditions for each lane are described in the text. Super: supercomplex consisting of I_1, III_2, and IV_1, which are complex I monomer, complex III dimer, and CcO monomer, respectively. Each of these is a functional unit.

monomer, the complexes I, III dimer, and V, but little of the CcO dimer. The solutions with digitonin and LMNG also contain the supercomplex, in which the CcO monomer and complexes I and III dimer are associated with each other.

To purify CcO for crystallization, the KHP homogenate is solubilized by using 3.8% (w/v) sodium cholate. Subsequently, CcO was fractionated by AS precipitation first with cholate four times and then with alkyl glycoside detergent three times. In the first fractionation, immediately after solubilization, AS is added to 33% saturation at pH 7.3–7.4 while stirring for 30 min, followed by centrifugation. AS is added to the supernatant to 50% saturation, and the centrifuge precipitate is dissolved in 220 mL buffer with 0.5% (w/v) sodium cholate. The solution contains large amounts of CcO dimer, complexes I, III dimer, and V, but a small amount of CcO monomer (Fig. 2B, lane 1). The solution is dialyzed against 40 mM Na-Pi for 90 min, followed by ultra-centrifugation. The precipitates are re-solubilized in 200 mL buffer with 2.0% (w/v) sodium cholate. Complex V is excluded from the sample, whereas most of the CcO remains as the dimer (Fig. 2B, lane 2). In the second fractionation, AS is added to 25% saturation at pH 7.3–7.4 with stirring for 20 min, followed by centrifugation. AS is added to the supernatant to 45% saturation, and the centrifuge precipitates are dissolved in 200 mL buffer with 0.5% (w/v) sodium cholate. Complex III is excluded from the solution, whereas most of the CcO remains as the dimer (Fig. 2B, lane 3). In the third fractionation, AS precipitation is performed from 25% to 40% saturation. The precipitates are dissolved in 130 mL buffer with 0.5% (w/v) sodium cholate. Complex I is excluded from the sample, and the sample solution contains dimeric CcO and more than 1000 cholate molecules per CcO molecule (Fig. 2B, lane 4; Table 1, line 1). In the fourth fractionation, AS precipitation is performed from 25% to 35% saturation. The precipitates are then dissolved in 200 mL buffer with 0.34% (w/v) DM or 0.2% (w/v) 3-oxatridecyl-α-$_D$-mannoside (3OM). In the fifth fractionation, AS precipitation without stirring is performed from 40% to 60% saturation with DM, or from 35% to 55% saturation with 3OM. In the DM sample, the amount of cholate decreases to about 400 molecules/CcO (Table 1, line 2), and the quantitative ratio of monomeric CcO increases (Fig. 2B, lane 5). The precipitates are dissolved in 100 mL buffer with 0.2% (w/v) DM or 3OM, and stored. In the sixth fractionation, after adjusting the volume to 220 mL, AS precipitation is performed from 50% to 70% saturation with DM, or from 40% to 60% saturation with 3OM. The precipitates are dissolved in 200 mL buffer with 0.2% (w/v) DM or 3OM. In the seventh fractionation, AS precipitation is performed from 55% to 70% saturation with DM, or from 45% to 70% saturation with 3OM. The CcO precipitates are dissolved in 10–15 mL buffer with 0.2% (w/v) DM or 15–20 mL buffer with 0.2%

Table 1   Change in the number of cholate molecules per CcO molecule during purification

Purification step	Cholate/CcO (mol/mol)
Third fractionation	1050.2
Fifth fractionation	382.6
After dialysis	32.5
Microcrystals	14.1

Data are from [2].

(w/v) 3OM. After the fractionation, the DM and 3OM samples are dialyzed against 10 mM Na-Pi buffer (pH 7.4) and 50 mM Na-Pi buffer (pH 6.2), respectively. About 800 mg of purified CcO is obtained from 1100 g of bovine heart. In the DM sample, the amount of cholate is decreased to about 30 molecules/CcO (Table 1, line 3), and almost all the CcO molecules are monomers (Fig. 2B, lane 6).

For crystallization with 3OM, the sample is concentrated to 80–90 mg protein/mL by ultrafiltration, and PEG 4000 is added as a precipitant. Crystallization is performed by the batch method, and the solution is placed on a concave microscope slide covered with a coverslip. Monomeric CcO crystals grow within 1–2 weeks. For crystallization with DM, the sample is washed (ultrafiltration and dilution) four times. In the first wash, the sample is diluted with 20 mM Na-Pi buffer (pH 7.4) containing 0.2% (w/v) DM. In the second to fourth washes, the sample is diluted by 40 mM Na-Pi buffer (pH 6.8) with 0.2% (w/v) DM. Finally, the sample is concentrated to 140 mg protein/mL or higher. In this sample, CcO forms a dimer again (Fig. 2B, lane 7), and dimeric CcO microcrystals grow (Fig. 2B, lane 8). The amount of cholate in the microcrystals is 14 molecules/CcO (Table 1, line 4). After addition of PEG 4000 as a precipitant, crystallization is performed by the batch method, and the solution is placed on a concave microscope slide covered with a coverslip. Dimeric CcO crystals grow within 2–5 days.

Further properties of the dimerization/monomerization of the DM sample are shown in Figure 2C. The CcO dimer is stable in the microcrystal solution at a concentration of at least 15 mg/mL and pH 6.8 (Fig. 2C, lane 1); however, the CcO monomer appears when the CcO concentration is reduced to 1.5 mg/mL at pH 6.8, (Fig. 2C, lane 2). Gel filtration chromatography shows that monomerization happens due to a further decrease in CcO concentration [8]. Monomerization of 1.5 mg/mL CcO sample occurs when the pH is raised to 8.5 (Fig. 2C, lane 3) or 7.4 (Fig. 2C, lane 4). These results suggest that CcO in the DM sample is in an equilibrium state between the dimer and monomer.

The properties of purified CcO can be evaluated by cytochrome *c* oxidation activity. However, because the activity measurement is usually performed at a low CcO
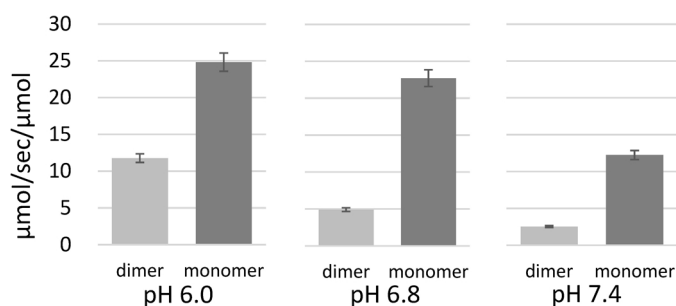
Figure 3 Ferrocytochrome *c* oxidation activity at 20°C. The concentrations of ferrocytochrome *c* and CcO are 10 μM and 4.8 nM, respectively. Figure reproduced from [8].

concentration, only monomeric CcO is present, and thus it has been difficult to compare the CcO activity between monomeric and dimeric states. This problem was solved by using a new type of sample, in which an amphipol stabilizes each CcO dimer (Fig. 2D, lane 1) and CcO monomer (Fig. 2D, lane 2). The sample is prepared as follows (details of preparation methods are described in [8]). Amphipol is added to the CcO dimer solution with DM or to the CcO monomer solution with octyl glucopyranoside. The detergents are removed from the sample using cyclodextrin, and the CcO monomer and dimer are collected by sucrose density gradient centrifugation without DM. Figure 3 shows that the activity of the amphipol-stabilized CcO monomer is higher than that of the dimer, indicating that the monomeric form is the physiologically active form. The pH dependence of the activity is essentially the same as that of detergent solubilized CcO. The CcO monomer and dimer are still stable after the measurement.

Crystallographic analysis of monomeric and dimeric CcO

To understand the transition mechanism and the activity difference between monomeric and dimeric CcO based on the molecular structure, crystallographic analyses have been performed using crystals consisting of CcO monomer with 3OM at 1.85 Å resolution (Fig. 4A) [8], and CcO dimer with DM at 1.3 Å resolution (Fig. 4B) [2]. Structural comparison shows that the core region (subunits I, II, and III) is similar in the monomeric and dimeric structures; however, there are major differences in the peripheral regions involved in monomer-monomer association in the dimer and in the crystal packing between the monomeric and dimeric structures (Fig. 4C).

Figure 5A shows part of the dimer interface consisting of the transmembrane helices of subunits I and II in one monomer and the transmembrane helix of subunit VIa in the other monomer, where the clear electron density of the cholate molecule (CH2) is observed. In contrast, CH2 is completely absent from the monomeric form. CH2 is stabilized by two hydrogen bonds with Glu62[II] and Thr63[II] and one hydrophobic interaction with Trp275[I] in one monomer, and four hydrogen bonds with Arg14[VIa] and Arg17[VIa] and one hydrophobic interaction with Phe18[VIa] in the other monomer. Together with biochemical evidence of the effect of cholate on the dimerization shown in Figure 2, these findings imply that the binding of CH2 triggers dimerization. This is consistent with previous biochemical reports, in which cholate and its analogues, deoxy-cholate and 3-[(3-cholamidopropyl)dimethylammonio]-1-propanesulfonate (CHAPS), induced dimerization of monomeric CcO solubilized with DDM or a phospholipid [34,35]. The electron density of the segment containing Glu62[II] is reduced in monomeric CcO, meaning that this segment structure is unstable in the monomer compared with the dimer. Moreover, a water molecule (Wat2) is positioned in monomeric CcO where there is a Glu62[II] carboxyl group in dimeric CcO (Fig. 5B). In monomeric CcO, Wat2 forms part of a hydrogen bond network of water molecules (Wat1–Wat4) and Met273[I] in the K-pathway. However, in dimeric CcO, this hydrogen bond network is broken, because Wat2 is replaced by a Glu62[II] carboxyl group that is hydrogen bonded to Wat1 and CH2 (Fig. 5C). These structural differences suggest that the hydrogen bond network in the monomeric structure enables the uptake of protons, whereas CH2 binding in the dimeric structure inhibits proton uptake. Accordingly, the difference in activity between monomeric and dimeric CcO may be due to the structural difference of hydrogen bond network in the K-pathway caused by binding of CH2. This is consistent with the known inhibition of bovine CcO activity by cholate [36,37].

Besides the K-pathway entrance, monomeric and dimeric structure show no major differences in other functionally important sites (i.e., cytochrome *c*–binding site, heme a_3–Cu_B site, O_2-transfer channel, and the D- and H-pathways for proton transfer). Previously determined structures indicate that even when CcO is dimerized, each of these sites can be accessed with a specific substrate
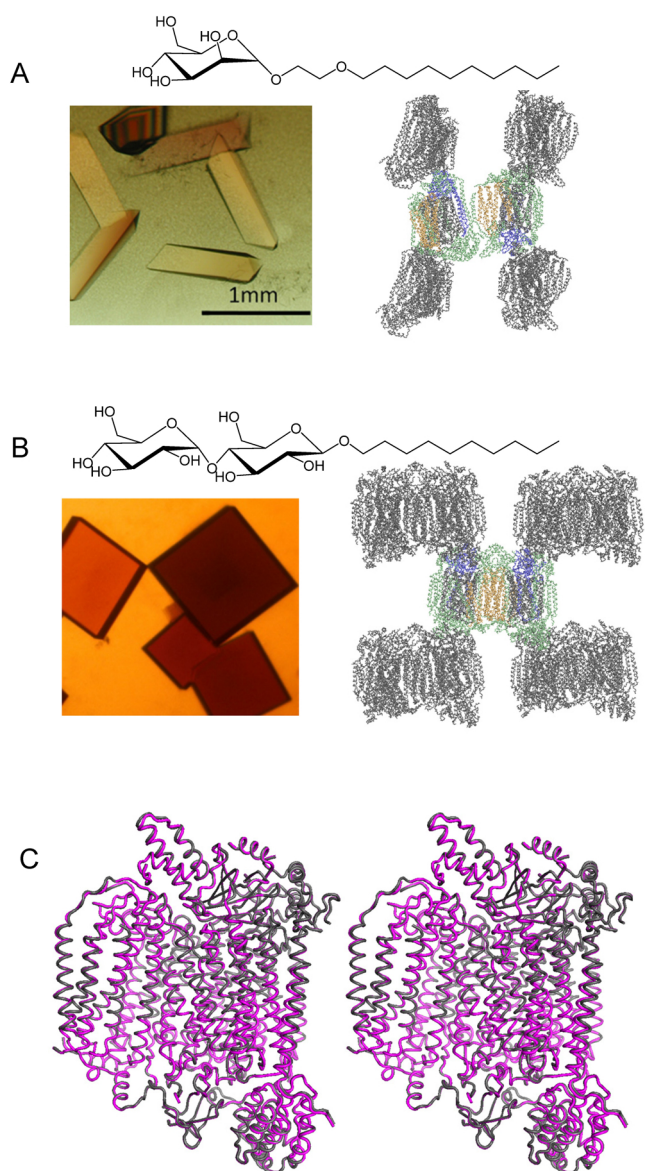
Figure 4 Detergents, CcO crystals, and crystal structures. Subunits I and II, and other subunits in CcO in the central position are shown in gray, light blue, and green, respectively. (A) 3OM, monomeric CcO crystals with 3OM, and crystal structure from [PDB ID: 6JY3] [32]. Picture of crystals reproduced from [8]. (B) DM, dimeric CcO crystals with DM, and crystal structure from [PDB ID: 7COH] [33]. (C) Stereo view of the superposition of the monomeric CcO structure (magenta) and one monomer structure of dimeric CcO (gray).

Figure 5 (A) Structure of the CcO dimer interface [PDB ID: 7COH] [33]. The molecular surfaces of the two monomers in dimeric CcO are shown in gray and green. The amino acid residues involved in the dimerization are shown as stick models, in which the carbon atoms are cyan. (B, C) Proton transfer K-pathways in (B) the monomeric CcO structure [PDB ID: 6JY3] [32] and (C) one monomer structure of dimeric CcO [PDB ID: 7COH] [33]. The molecular surfaces of subunits I and II, and other subunits are shown in gray, light blue, and cyan, respectively. The amino acid residues and water molecules in the K-pathway are shown as stick and ball models, respectively. Each water molecule is numbered from 1 to 4.

(electron donor, O_2, or proton), implying that these sites function in both monomeric and dimeric forms. Previous structural analyses of dimeric CcO have revealed that several regions in subunits I and II change their conformation depending on the redox state of CcO [10,38,39]. These structural changes may be involved in the enzymatic function. The same redox-dependent changes are observed in monomeric CcO, indicating that the activity
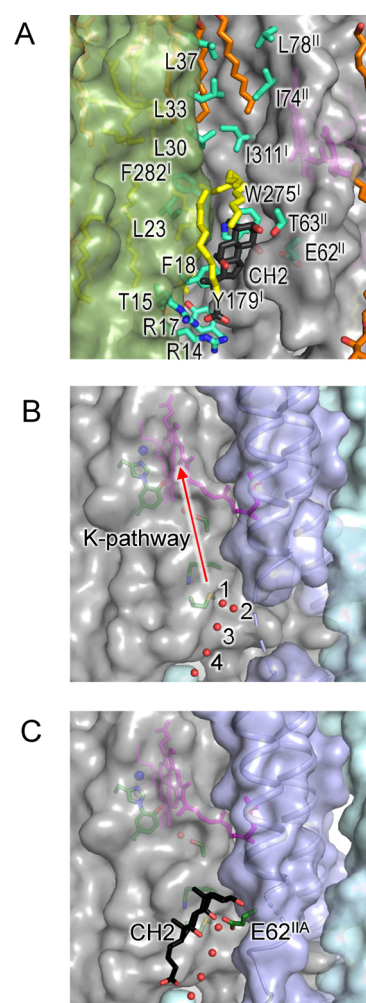
difference between monomeric and dimeric CcO does not depend on these structural changes. These results indicate that a difference in proton uptake function at the entrance of the K-pathway is the sole difference affecting the activity between the monomer and dimer, and the monomeric structure shown here is an active form of CcO.

In the 1.3 Å resolution structure of dimeric CcO, there are many long, thin electron densities on the trans-membrane surface, although most of the densities are low. Among these electron densities, 13 hydrocarbon tail fragments of unidentified lipids and seven DMs have been

modeled at the dimer interface (Figs. 6A and 6B). No clear electron density for the phospholipid head group or the difference electron density for the phosphorus atom is observed at the dimer interface. Therefore, part of the dimer interface consists of non-specifically bound lipids that can be replaced by detergent. In addition to these lipid fragments and detergents, the electron density for another cholate molecule (CH1) is clearly visible at the dimer interface (Fig. 6B). CH1 is stabilized by five hydrogen bonds with one monomer and one hydrophobic interaction (3.7 Å distance) with the other monomer, meaning that CH1 is more tightly bound to one monomer than the other. Some of these electron densities are also observed on the surface of monomeric CcO, although the resolution at 1.85 Å is not sufficient for modeling, except for CH1. CH1 is stabilized in monomeric CcO in the same manner as in one monomer of dimeric CcO. On the opposite side of the dimer interface, the anomalous difference electron densities of phosphorus atoms are observed in both monomeric and dimeric CcO structures. Based on the electron density shapes and anomalous peak positions, these phosphorus atoms are identified as elements of three cardiolipins (CLs; CL2, CL3, and CL4) bound to the transmembrane surface. Both monomeric and dimeric CcOs show similar electron density properties at the tails of the CLs, where electron density is low in several terminal segments. Current monomeric and dimeric CcO models contain eight 3OM binding sites and 17 DM binding sites, respectively, in which five sites are common for 3OM and DM (Fig. 6B). Four DMs and three 3OMs are observed on the transmembrane surface of subunit III, where the entrance of the O$_2$ transfer channel is formed.

Formation of the monomer, dimer, and supercomplex

Based on the comparison of the monomeric and dimeric structures, the following three factors are crucial for the dimerization: cholate binding, especially CH2 between the transmembrane helices at the dimer interface near the K-pathway; hydrophobic interactions of the lipid (detergent) tails sandwiched between monomers in the dimer; and peptide-peptide interactions between the transmembrane helices and between the extramembrane regions. The CH2 binding site is formed with several hydrogen bonds, implying that this site is specific for binding cholate. Therefore, the binding of physiological ligands that are a similar molecular size or shape to cholate could also trigger dimerization in the mitochondrial membrane. We have examined the effect of ATP, ADP, or cholesterol on the mitochondrial fractions solubilized with LMNG or DM; however, we did not observe an obvious effect indicating dimerization [2]. The hydrophobic interactions of the lipid (detergent) tails are not strong because their electron
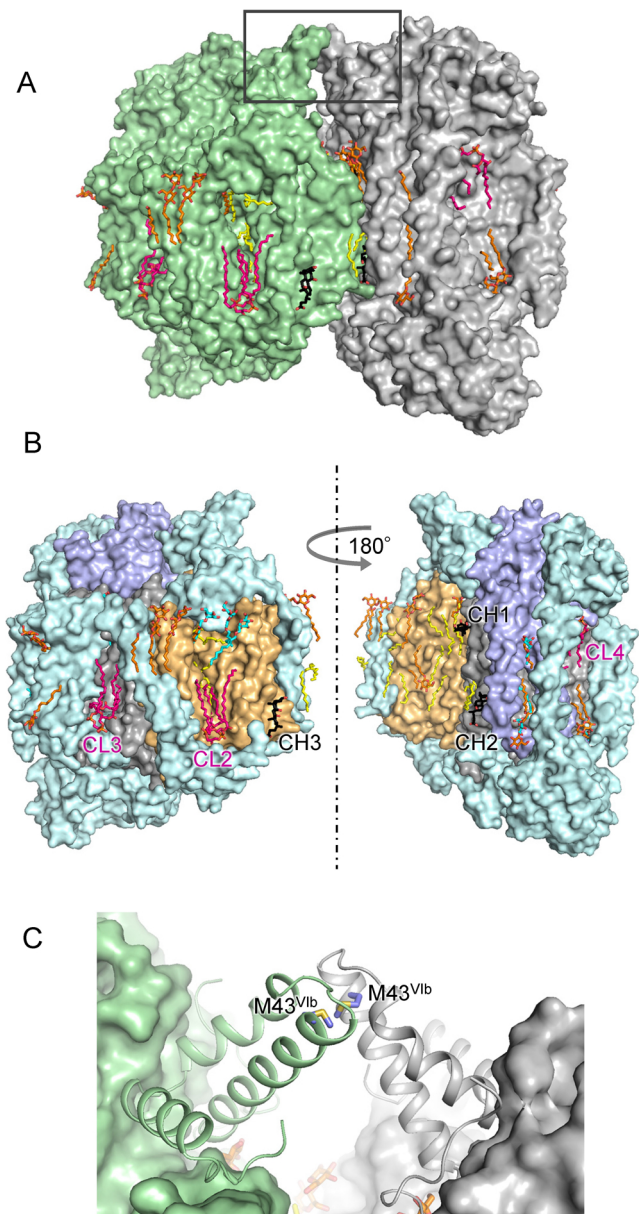

Figure 6　(A) Whole structure of dimeric CcO [PDB ID: 7COH] [33]. The molecular surfaces of the two monomers in dimeric CcO are shown in gray and green. The lipid, DM, and cholate (black) molecules are shown as stick models. The carbon atoms in CLs, other lipids, and DMs are shown in magenta, yellow, and orange, respectively. (B) Structure of one monomer in dimeric CcO [PDB ID: 7COH] [33]. Molecular surfaces of subunits I and II, and other subunits are shown in gray, light blue, and cyan, respectively. 3OM molecules from [PDB ID: 6JY3] [32], in which the carbon atoms are shown in cyan, are superposed. (C) Close-up view of the upper part of dimeric CcO in panel A. The VIb subunits in each monomer are shown as cartoon models. Met43 in each subunit VIb is shown as a stick model.

densities are weak. In a physiological environment, non-specifically bound lipids could support the stabilization of the dimeric form. The peptide-peptide interactions between
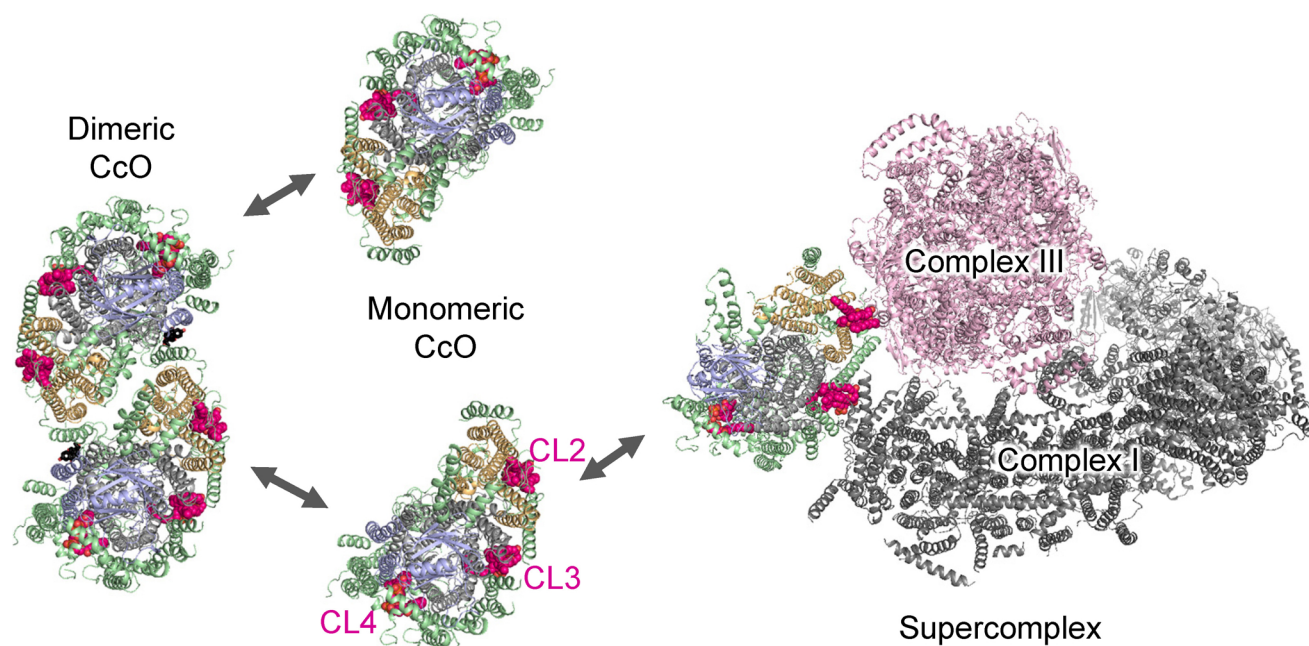
Figure 7   Structures of CcO in the dimer [PDB ID: 7COH] [33], monomer [PDB ID: 6JY3] [32], and supercomplex states (CcO from [PDB ID: 6JY3] [32], and complexes I and III from [PDB ID: 5J4Z] [40]). Subunits I and II, and other subunits in CcO are shown in gray, light blue, and green, respectively. CLs are shown in magenta. Complexes I and III are shown in yellow and pink, respectively.

the transmembrane helices involve four leucine residues of subunit VIa (Leu37, Leu33, Leu30, and Leu23) and residues of subunits I and II (Leu78^{II}, Ile74^{II}, Ile311^{I}, and Phe282^{I}) in another monomer (Fig. 5A). These hydrophobic interactions may be stabilized by CH2 binding, and a hydrogen bond between Thr15^{VIa} and Tyr179^{I} in another monomer. The peptide-peptide interactions in the extramembrane region involve the VIb subunits of each monomer (Fig. 6C). The interface consists of parallel backbones of the loop segments of (Lys46–Gly47–Gly48–Asp49)^{VIb}, and a Met–Met interaction between the Met43 in each subunit VIb. These interactions are weak relative to a typical hydrogen bond interaction, but may play a role in correcting the orientation of the two monomers.

The comparison of monomeric and supercomplex structures suggests that CLs are involved in the association of CcO in the supercomplex. When our CcO structure is superposed onto the supercomplex structure determined by cryo-electron microscopy, CL3 is located between CcO and complex I, and CL2 is located between CcO and complex III (Fig. 7). The terminal segments of these CL tails show low electron densities, implying conformational flexibility; therefore, these segments could interact with the transmembrane regions of complexes I and III, and play a role in stabilizing the supercomplex. This is consistent with the findings of biochemical studies and computer simulations for mitochondrial enzymes, and cryo-electron microscopy structural analysis for mycobacterium

enzymes, in which cardiolipin is involved in the supercomplex formation [23,24,41,42]. Therefore, it is expected that CL-mediated supercomplex formation is universal across species. In the bovine mitochondrial membrane, complexes I and III and CcO are present in the ratio 1:3:6–7. This implies that not all CcOs are involved in forming the supercomplex, in which the ratio of complexes I and III, and CcO is 1:2:1. Other CcOs should be present in monomeric or dimeric form, as shown by mass spectroscopic analysis [19]. When the mitochondrial membrane is solubilized, the amount of monomer is much larger than that of the dimer, whereas dimerization depends on the cholate and enzyme concentrations and pH (Fig. 2). Dimerization is also caused by the addition of cholate analogs [34,35], or by reconstitution of CcO into mixed-lipid liposomes [18]. Based on these results, we postulate that in the mitochondrial membrane, CcO is in equilibrium between the independent monomer, the monomer in the supercomplex, and the dimer. The activity of CcO may be regulated by the transition among these states that is trigged by some physiological ligands or conditions.

Acknowledgement

Conflicts of Interest

K.S.-I. and K.M. declare that they have no conflict of interest.

Author Contribution

K.S.-I. and K.M. wrote this review article.

References

[1] Tsukihara, T., Aoyama, H., Yamashita, E., Tomizaki, T., Yamaguchi, H., Shinzawa-Itoh, K., et al. The whole structure of the 13-subunit oxidized cytochrome c oxidase at 2.8 A. Science 272, 1136–1144 (1996). DOI: 10.1126/science.272.5265.1136

[2] Shinzawa-Itoh, K., Hatanaka, M., Fujita, K., Yano, N., Ogasawara, Y., Iwata, J., et al. The 1.3-Å resolution structure of bovine cytochrome c oxidase suggests a dimerization mechanism. BBA Adv. 1, 100009 (2021). DOI: 10.1016/j.bbadva.2021.100009

[3] Muramoto, K., Ohta, K., Shinzawa-Itoh, K., Kanda, K., Taniguchi, M., Nabekura, H., et al. Bovine cytochrome c oxidase structures enable O_2 reduction with minimization of reactive oxygens and provide a proton-pumping gate. Proc. Natl. Acad. Sci. USA 107, 7740–7745 (2010). DOI: 10.1073/pnas.0910410107

[4] Ishigami, I., Lewis-Ballester, A., Echelmeier, A., Brehm, G., Zatsepin, N. A., Grant, T. D., et al. Snapshot of an oxygen intermediate in the catalytic reaction of cytochrome c oxidase. Proc. Natl. Acad. Sci. USA 116, 3572–3577 (2019). DOI: 10.1073/pnas.1814526116

[5] Shimada, A., Etoh, Y., Kitoh-Fujisawa, R., Sasaki, A., Shinzawa-Itoh, K., Hiromoto, T., et al. X-ray structures of catalytic intermediates of cytochrome c oxidase provide insights into its O_2 activation and unidirectional proton-pump mechanisms. J. Biol. Chem. 295, 5818–5833 (2020). DOI: 10.1074/jbc.RA119.009596

[6] Shimada, S., Shinzawa-Itoh, K., Baba, J., Aoe, S., Shimada, A., Yamashita, E., et al. Complex structure of cytochrome c-cytochrome c oxidase reveals a novel protein-protein interaction mode. EMBO J. 36, 291–300 (2017). DOI: 10.15252/embj.201695021

[7] Muramoto, K., Hirata, K., Shinzawa-Itoh, K., Yoko-o, S., Yamashita, E., Aoyama, H., et al. A histidine residue acting as a controlling site for dioxygen reduction and proton pumping by cytochrome c oxidase. Proc. Natl. Acad. Sci. USA 104, 7881–7886 (2007). DOI: 10.1073/pnas.0610031104

[8] Shinzawa-Itoh, K., Sugimura, T., Misaki, T., Tadehara, Y., Yamamoto, S., Hanada, M., et al. Monomeric structure of an active form of bovine cytochrome c oxidase. Proc. Natl. Acad. Sci. USA 116, 19945–19951 (2019). DOI: 10.1073/pnas.1907183116

[9] Shinzawa-Itoh, K., Aoyama, H., Muramoto, K., Terada, H., Kurauchi, T., Tadehara, Y., et al. Structures and physiological roles of 13 integral lipids of bovine heart cytochrome c oxidase. EMBO J. 26, 1713–1725 (2007). DOI: 10.1038/sj.emboj.7601618

[10] Yano, N., Muramoto, K., Shimada, A., Takemura, S., Baba, J., Fujisawa, H., et al. The Mg^{2+}-containing water cluster of mammalian cytochrome c oxidase collects four pumping proton equivalents in each catalytic cycle. J. Biol. Chem. 291, 23882–23894 (2016). DOI: 10.1074/jbc.M115.711770

[11] Shimokata, K., Katayama, Y., Murayama, H., Suematsu, M., Tsukihara, T., Muramoto, K., et al. The proton pumping pathway of bovine heart cytochrome c oxidase. Proc. Natl. Acad. Sci. USA 104, 4200–4205 (2007). DOI: 10.1073/pnas.0611627104

[12] Yoshikawa, S. & Shimada, A. Reaction mechanism of cytochrome c oxidase. Chem. Rev. 115, 1936–1989 (2015). DOI: 10.1021/cr500266a

[13] Maréchal, A., Xu, J-Y., Genko, N., Hartley, A. M., Haraux, F., Meunier, B., et al. A common coupling mechanism for A-type heme-copper oxidases from bacteria to mitochondria. Proc. Natl. Acad. Sci. USA 117, 9349–9355 (2020). DOI: 10.1073/pnas.2001572117

[14] Sousa, F. L., Alves, R. J., Ribeiro, M. A., Pereira-Leal, J. B., Teixeira, M. & Pereira, M. M. The superfamily of heme-copper oxygen reductases: types and evolutionary considerations. Biochim. Biophys. Acta Bioenerg. 1817, 629–637 (2012). DOI: 10.1016/j.bbabio.2011.09.020

[15] Wikström, M., Krab, K. & Sharma, V. Oxygen activation and energy conservation by cytochrome c oxidase. Chem. Rev. 118, 2469–2490 (2018). DOI: 10.1021/acs.chemrev.7b00664

[16] Gopalasingam, C. C., Johnson, R. M., Chiduza, G. N., Tosha, T., Yamamoto, M., Shiro, Y., et al. Dimeric structures of quinol-dependent nitric oxide reductases (qNORs) revealed by cryo-electron microscopy. Sci. Adv. 5, eaax1803 (2019). DOI: 10.1126/sciadv.aax1803

[17] Jamali, M. A. M., Gopalasingam, C. C., Johnson, R. M., Tosha, T., Muramoto, K., Muench, S. P., et al. The active form of quinol-dependent nitric oxide reductase from Neisseria meningitidisis a dimer. IUCrJ 7, 404–415 (2020). DOI: 10.1107/s2052252520003656

[18] Rubinson, K. A., Pokalsky, C., Krueger, S. & Prochaska, L. J. Structure determination of functional membrane proteins using small-angle neutron scattering (SANS) with small, mixed-lipid liposomes: native beef heart mitochondrial cytochrome c oxidase forms dimers. Potein J. 32, 27–38 (2013). DOI: 10.1007/s10930-012-9455-0

[19] Chorev, D. S., Baker, L. A., Wu, D., Beilsten-Edmands, V., Rouse, S. L, Zeev-Ben-Mordehai, T., et al. Protein assemblies ejected directly from native membranes yield complexes for mass spectrometry. Science 362, 829–834 (2018). DOI: 10.1126/science.aau0976

[20] Letts, J. A., Fiedorczuk, K. & Sazanov, L. A. The architecture of respiratory supercomplexes. Nature 537, 644–648 (2016). DOI: 10.1038/nature19774

[21] Wu, M., Gu, J., Guo, R., Huang, Y. & Yang, M. Structure of mammalian respiratory supercomplex $I_1III_2IV_1$. Cell 167, 1598–1609.e10 (2016). DOI: 10.1016/j.cell.2016.11.012

[22] Rathore, S., Berndtsson, J., Marin-Buera, L., Conrad, J., Carroni, M., Brzezinski, P., et al. Cryo-EM structure of the yeast respiratory supercomplex. Nat. Struct. Mol. Biol. 26, 50–57 (2019). DOI: 10.1038/s41594-018-0169-7

[23] Gong, H., Li, J., Xu, A., Tang, Y., Ji, W., Gao, R., et al. An electron transfer path connects subunits of a mycobacterial respiratory supercomplex. Science 362, eaat8923 (2018).

DOI: 10.1126/science.aat8923

[24] Wiseman, B., Nitharwal, R. G., Fedotovskaya, O., Schäfer, J., Guo, H., Kuang, Q., *et al.* Structure of a functional obligate complex III$_2$IV$_2$ respiratory supercomplex from *Mycobacterium smegmatis*. *Nat. Struct. Mol. Biol.* **25**, 1128–1136 (2018). DOI: 10.1038/s41594-018-0160-3

[25] Kadenbach, B. & Hüttemann, M. The subunit composition and function of mammalian cytochrome *c* oxidase. *Mitochondrion* **24**, 64–76 (2015). DOI: 10.1016/j.mito.2015.07.002

[26] Chaban, Y., Boekema, E. J. & Dudkina, N. V. Structures of mitochondrial oxidative phosphorylation supercomplexes and mechanisms for their stabilisation. *Biochim. Biophys. Acta* **1837**, 418–426 (2014). DOI: 10.1016/j.bbabio.2013.10.004

[27] Genova, M. L. & Lenaz, G. Functional role of mitochondrial respiratory supercomplexes. *Biochim. Biophys. Acta Bioenerg.* **1837**, 427–443 (2014). DOI: 10.1016/j.bbabio.2013.11.002

[28] Acín-Pérez, R. & Enríquez, J. A. The function of the respiratory supercomplexes: The plasticity model. *Biochim. Biophys. Acta Bioenerg.* **1837**, 444–450 (2014). DOI: 10.1016/j.bbabio.2013.12.009

[29] Shinzawa-Itoh, K., Shimomura, H., Yanagisawa, S., Shimada, S., Takahashi, R., Oosaki, M., *et al.* Purification of active respiratory supercomplex from bovine heart mitochondria enables functional studies. *J. Biol. Chem.* **291**, 4178–4184 (2016). DOI: 10.1074/jbc.M115.680553

[30] Moe, A., Di Trani, J., Rubinstein, J. L. & Brzezinski, P. Cryo-EM structure and kinetics reveal electron transfer by 2D diffusion of cytochrome *c* in the yeast III-IV respiratory supercomplex. *Proc. Natl. Acad. Sci. USA* **118**, e2021157118 (2021). DOI: 10.1073/pnas.2021157118

[31] Schägger, H. & von Jagow, G. Blue native electrophoresis for isolation of membrane protein complexes in enzymatically active form. *Anal Biochem.* **199**, 223–231 (1991). DOI: 10.1016/0003-2697(91)90094-a

[32] Shinzawa-Itoh, K. & Muramoto, K. Monomeric form of bovine heart cytochrome *c* oxidase in the fully oxidized state. Protein Data Bank. https://pdbj.org/mine/summary/6jy3. Deposited 26 April 2019.

[33] Shinzawa-Itoh, K., Muramoto, K. Dimeric form of bovine heart cytochrome *c* oxidase in the fully oxidized state. Protein Data Bank. https://pdbj.org/mine/summary/7coh. Deposited 4 August 2020.

[34] Musatov, A., Ortega-Lopez, J. & Robinson, N. C. Detergent-solubilized bovine cytochrome *c* oxidase: dimerization depends on the amphiphilic environment. *Biochemistry* **39**, 12996–13004 (2000). DOI: 10.1021/bi000884z

[35] Musatov, A. & Robinson, N. C. Cholate-induced dimerization of detergent- or phospholipid-solubilized bovine cytochrome *c* oxidase. *Biochemistry* **41**, 4371–4376 (2002). DOI: 10.1021/bi016080g

[36] Van Buuren, K. J. & Van Gelder, B. F. Biochemical and biophysical studies on cytochrome *c* oxidase. XIII. Effect of cholate on the enzymic activity. *Biochim. Biophys. Acta Bioenerg.* **333**, 209–217 (1974). DOI: 10.1016/0005-2728(74)90005-x

[37] Sinjorgo, K. M. C., Durak, I., Dekker, H. L., Edel, C. M., Bieleman, A. H. L., Back, N. B. T., *et al.* The effect of detergents on bovine cytochrome *c* oxidase: A kinetic approach. *Biochim. Biophys. Acta Bioenerg.* **893**, 241–250 (1987). DOI: 10.1016/0005-2728(87)90045-4

[38] Yoshikawa, S., Shinzawa-Itoh, K., Nakashima, R., Yaono, R., Yamashita, E., Inoue, N., *et al.* Redox-coupled crystal structural changes in bovine heart cytochrome *c* oxidase. *Science* **280**, 1723–1729 (1998). DOI: 10.1126/science.280.5370.1723

[39] Tsukihara, T., Shimokata, K., Katayama, Y., Shimada, H., Muramoto, K., Aoyama, H., *et al.* The low-spin heme of cytochrome *c* oxidase as the driving element of the proton-pumping process. *Proc. Natl. Acad. Sci. USA* **100**, 15304–15309 (2003). DOI: 10.1073/pnas.2635097100

[40] Letts, J. A., Fiedorczuk, K., Sazanov, L. A. Architecture of tight respirasome. Protein Data Bank. https://pdbj.org/mine/summary/5j4z. Deposited 1 April 2016.

[41] Mileykovskaya, E. & Dowhan, W. Cardiolipin-dependent formation of mitochondrial respiratory supercomplexes. *Chem. Phys. Lipids* **179**, 42–48 (2014). DOI: 10.1016/j.chemphyslip.2013.10.012

[42] Arnarez, C., Marrink, S. J. & Periole, X. Molecular mechanism of cardiolipin-mediated assembly of respiratory chain supercomplexes. *Chem. Sci.* **7**, 4435–4443 (2016). DOI: 10.1039/c5sc04664e

(*Edited by Haruki Nakamura*)